

Recurrent Human Pose Estimation

Vasileios Belagiannis and Andrew Zisserman

University of Oxford
Department of Engineering Science, UK
vb,az@robots.ox.ac.uk

Abstract. We propose a novel ConvNet model for predicting 2D human body poses in an image. The model regresses a heatmap representation for each body keypoint, and is able to learn and represent both the part appearances and the context of the part configuration.

We make the following three contributions: (i) an architecture combining a feed forward module with a recurrent module, where the recurrent module can be run iteratively to improve the performance; (ii) the model can be trained end-to-end and from scratch, with auxiliary losses incorporated to improve performance; (iii) we investigate whether keypoint visibility can also be predicted.

The model is evaluated on two benchmark datasets. The result is a simple architecture that achieves performance on par with the state of the art, but without the complexity of a graphical model stage (or layers).

1 Introduction

Estimating 2D human pose from images is a challenging task with many applications in computer vision, such as motion capture, sign language and activity recognition. For many years approaches have used variations on the pictorial structure model [13,15] of a combination of part detectors and configuration constraints [2,14,25,29,39]. However, the advent of ConvNets, together with large scale training sets, has led to models that perform well in demanding scenarios with unconstrained body postures and large appearance variations [9,32,34]. As the individual part detectors, e.g. the hand and limb detectors, and the pairwise part detectors have become stronger, so the importance of the configuration constraints has begun to wane, with quite recent methods not even including an explicit graphical model [4,8,22].

Nevertheless, performance has not saturated yet – the best recent methods (one of which includes an explicit graphical model in the ConvNet layers) ‘only’ achieve a PCKh score in the 80s on the MPII Human Pose [1] database test-set. This is a remarkable improvement over methods from two years ago, but it has still not reached the high 90s.

In this paper, we describe a new ConvNet model and training scheme for human pose estimation that makes the following contributions: (i) a model combining a feed forward module with a recurrent module, where the recurrent module can be run iteratively to improve the performance (see Fig. 1 and 5);

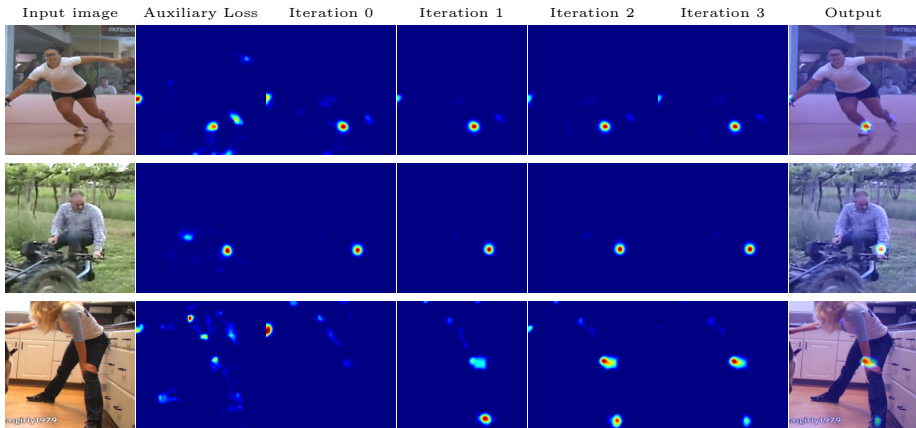


Fig. 1. Results of the Recurrent Human Model: The predicted heatmaps (MPII Human Pose dataset [1]) are visualized after every iteration of the recurrent module for the right ankle (*first row*), left wrist (*second row*) and left wrist (*third row*). Our model progressively suppresses false positive detections that occur at the first iterations.

(ii) the model can be trained end-to-end, and auxiliary losses can be incorporated to improve performance; and (iii) an investigation into improving occlusion predicting in human pose estimation.

Our model is mainly inspired by two recent papers: Pfister *et al.* [22] and Carreira *et al.* [8]. The first introduced the idea of ‘fusion layers’, convolutional layers that *implicitly* encode a configuration model. The second introduced an iterative update module which progressively makes incremental improvement to the pose estimate. We borrow the fusion layers idea from [22], but apply it multiple times as a recurrent network in the manner of [8]. However, unlike [8] our model is trained end-to-end, does not require a rendering function for combining the output with the input. There are also more technical improvements, that are described in detail in Section 2.

The outcome of our approach is a simple recurrent model that reaches state of the art performance on several standard benchmark datasets, but does not employ an explicit configuration model [9] nor a complicated network architecture [32].

1.1 Background and related work

For many years the ‘workhorse’ in human pose estimation has been a tree structured graphical model, often based on the efficient pictorial structure methods of Felzenszwalb and Huttenlocher [13]. This supported a host of methods, including [7,11,29,39]. An alternative approach, which also included configuration constraints, was based around the poselet idea [6,16].

Early methods using ConvNets predicted pose coordinates of human keypoints directly (as (x, y) coordinates) [34]. An alternative, which it turns out

might be better suited to ConvNets, is an indirect prediction by first regressing a heatmap over the image for each keypoint, and then obtaining the keypoint position as a mode in this heatmap [18,22,33,32]. The advantage of the heatmap over direct prediction is threefold: it mostly avoids problems with ConvNets predicting real values; it can handle multiple instances in the image (e.g. if there are several hands present and consequently several corresponding hand keypoints); and it can represent uncertainty by multiple modes.

The method of Carreira *et al.* [8] is an interesting hybrid that switches between regressing direct pose coordinates (as the output of the iterated module) and using a heatmap as the input (to the iterated module). In this respect it is similar to the architecture of [21] which also switches between direct pose coordinates and an image representation in an iterated module. In other related work, the iterated implicit configuration module of our model bears similarities to auto-context [35] and the message-passing inference machines of [27].

2 Recurrent Human Pose Model Architecture

Our aim is to predict 2D human body pose from a single image, represented as a set of keypoints. In this section we describe our ConvNet model that takes the image as input, and learns to regress a heatmap for each keypoint, where the location of the keypoint is obtained as a mode of the heatmap.

The architecture of the ConvNet is overviewed in Fig. 3. It consists of two modules: a *Feed-Forward module* that is run once, and a *Recurrent module* that can be run multiple times. Both modules output heatmaps, and can be trained with auxiliary losses. However, the key design idea of the architecture is how context is apportioned in training and inference. The Feed-Forward module mainly acts as an independent ‘part’ detector, regressing the keypoint heatmaps, but largely unaware of context from the configuration of other parts. In contrast the recurrent module progressively brings in more context each time it is run, in part because the effective receptive field is increased with each iteration (Fig. 1).

In the following we describe the architecture of the two modules and the loss function used for training. The entire network can be trained end-to-end, but we also describe the use of auxiliary losses that can be employed to speed up the training and improve performance. We also investigate two other aspects: the benefit of including additional supervision in the form of hallucinated annotation; and the benefit of training that is occlusion-aware.

2.1 Feed-forward Module

The module is based on the heatmap regression architecture of [22] with modifications. We use smaller filters (i.e. 3×3) for the initial convolutional layers, combined with non-linear activations (Layer 1 – 3 in Fig. 3). This idea from [30] allows more non-linearities to be included in the architecture, and leads to better performance. Pooling is applied only twice in order to retain the output heatmap

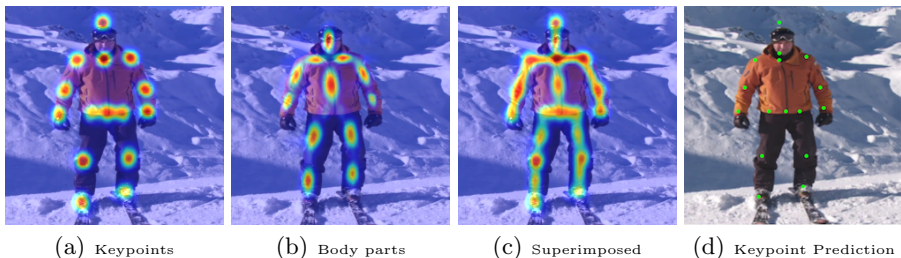


Fig. 2. Regressed Heatmaps: The regressed keypoint (a) and body part (b) heatmaps are presented for a validation sample. In (c), both heatmaps are superimposed, resulting in a human shape. The final outcome is the keypoint prediction (d), while the body part heatmaps act as an auxiliary task.

resolution sufficient large. The activation function is ReLU after every convolution and the prediction layers (Layer 8) are also convolutions that output the predicted heatmaps.

From Layer 4 to 6, larger convolution filters are employed to learn more of the body structure, followed by convolutions with 1×1 filters (Layer 5 and 7). The skip layer concatenates the output from Layer 3 and 5, which composes the input for the fusion layer [22] (Layer 6 and 7).

2.2 Recurrent Module

Our objective is to combine intermediate feature representations for learning context information and improving the final heatmap predictions. To that end, we introduce the recurrent module for the Layer 6 and 7 of our network. The input to the recurrent module is the concatenated output of Layer 3 and Layer 7. At every iteration, the input from Layer 3 is fixed, while Layer 7 is updated (see Fig. 3). Note that by using intermediate network layers for the recurrent module, we do not blend the predictions with the input, as in [8]. Finally, our network can be trained in an end-to-end fashion.

2.3 Body Part Heatmaps as Supplementary Supervision

Inspired by the idea of part-based models [2,3], we additionally propose body part heatmaps which are constructed by pairs of keypoints. In practice, we define the body part heatmap by taking the midpoint between the two keypoint as the center of the Gaussian distribution and define the variance based on the Euclidean distance between the two keypoints. Eventually, we model heatmaps for the body limbs, as it is depicted by Fig. 2. The keypoint heatmaps mostly represent body joints and the body part heatmap mainly capture limbs. Although, our main objective is to predict keypoints, modelling pairs of keypoints helps to capture additional body constraints and also acts as data augmentation, in terms of labels.

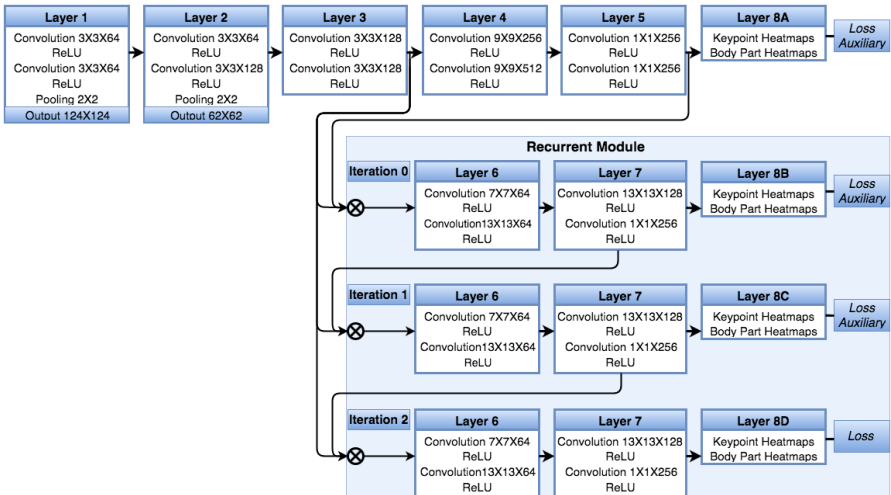


Fig. 3. ConvNet with Recurrent Module: Our network is composed of 7 layers. The recurrent model is introduced for Layer 6 and 7. In the current example, a network with 2 iterations is visualized. Note that all loss functions are auxiliary for facilitating the optimization and the final outcome comes from Layer 8D. Moreover, the body part heatmaps is an auxiliary task for additional data augmentation. In our graph, the symbol \otimes corresponds to the concatenation operation.

2.4 Target Heatmaps and Loss Function

At training time, the ground-truth labels are heatmaps synthesised for each keypoint separately by placing a Gaussian with fixed variance at the ground truth keypoint position. We then use an l_2 loss, which penalises the squared pixel-wise differences between the predicted heatmap and the synthesised ground-truth heatmap.

The same loss is also used for the feed-forward part and the recurrent module of the network. At every loss layer, we follow the same weighting that is 1 for the keypoint heatmaps and 0.1 for the body part heatmaps. Consequently, the gradients of the keypoint heatmaps have higher influence to the parameter update. Finally, the training of the ConvNet is accomplished using backpropagation [28] and stochastic gradient descent [5]. To hold down the computational load during training, the number of iterations is fixed, while additional iteration are added at test time to increase the accuracy of the heatmap predictions.

During training, Layer 8A is used as an auxiliary loss to comfort the optimization [31]. In addition, we propose to use an auxiliary loss function at the end of every iteration of the recurrent module, other than the last iteration, to boost the gradients' magnitude during backpropagation. As a result, Layer 8B and 8C are auxiliary tasks and the actual prediction is the outcome of Layer 8D, given a network of 2 iterations as in Fig. 3. Finally, the cost function of our

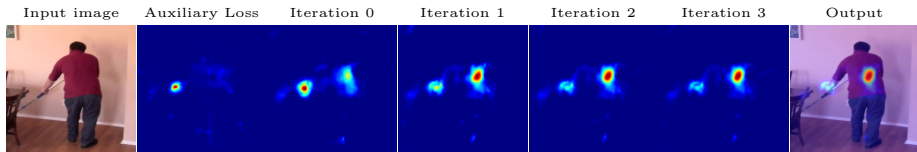


Fig. 4. Prediction of Ocluded Keypoints: The right wrist is erroneously predicted even though it is not visible because the model learns to capture context and it accordingly predicts. Note that occluded keypoints are not provided during training as ground-truth labels, instead they are ignored or penalized based on the occlusion scenario.

model for a set of S training samples is defined as:

$$E = \sum_{s=1}^S \|\mathbf{h}^s - f(\mathbf{x}, t; \boldsymbol{\theta})^s\|_2^2. \quad (1)$$

where \mathbf{h}^s is the synthesised ground-truth heatmap and $f(\cdot)$ represents the ConvNet with learned parameters $\boldsymbol{\theta}$ and the recurrent module at the t iteration.

2.5 Ocluded Keypoints

One of the most challenging aspects of predicting human body parts in images is dealing with the problem of occlusion – both self-occlusion and occlusion by other entities.

With the context carried by the recurrent module, we have a new way of approaching this problem. A body keypoint, such as a wrist, generates a strong response in a heatmap for two reasons: because the keypoint is visible and because it can be inferred from the configuration of the other keypoints of the body. The latter can potentially be a problem if configuration dominates over visibility, and a keypoint is predicted even though it is occluded (Fig. 4).

To this end, we investigate two training scenarios for the network: one *ignoring* occluded keypoints and body parts in the loss function (since they are not visible), and the other *penalizing* heatmaps that erroneously infer occluded parts at points predicted by context. In the first scenario, the gradient values of occluded keypoints or body parts are ignored at the respective heatmap areas during backpropagation (i.e. zero gradient). Thus, our network is trained without including occluded keypoints (i.e. noise) and at the same time without penalizing them. In the second scenario, the gradient values of occluded keypoints or body parts force the heatmap areas of the occluded parts to converge to zero. Fortunately, the MPII Human Pose dataset [1], which is used for training, provides occluded keypoint annotation within the context of predicted positions that can be used for this purpose.

3 Implementation Details

The network takes as input an RGB image with resolution 248×248 and outputs heatmaps with resolution a quarter of the input that is 62×62 . The input image is normalized by mean subtraction at each channel. Furthermore, data augmentation is performed by rotating, flipping and cropping the input image. Regarding the network parameters, the learning rate is set to 10^{-5} and gradually decreased to 10^{-6} , while we found that no more than 30 training epochs are required for obtaining a stable solution. Note that we train the model from scratch and the training time is less than 3 days. The momentum is set to 0.95 and the batch size to 20 samples. Also, batch normalization [17] is used for every convolutional layer other than the layers with 1×1 filters and the output layers.

The generated target heatmaps have σ variance set to 1.3 for the keypoint Gaussian distributions, while the body part heatmaps have different variance for the x and y direction based on the Euclidean distance between the two keypoints that form a part. In particular, we set σ_x and σ_y equal to 0.2 and 0.1 of the Euclidean distance. Moreover, we found it crucial to weight the gradients of the heatmaps, since the heatmap data is unbalanced. A heatmap has most of its area equal to zero (background) and only a small portion of it corresponds to the Gaussian distribution (foreground). For that reason, it is important to weight the gradient responses so that there is an equal contribution to the parameter update between the foreground and background heatmap pixels. Otherwise, there is a prior towards the background that forces the network to converge to zero. In addition, we magnify the Gaussian distributions so that their mode is around to 10 and consequently enlarge the difference between foreground and background pixels.

Furthermore a heatmap can include multiple individuals (e.g. MPII Human Pose dataset [1]). For our experiments, it is assumed that one is the active individual and the predictions of the rest are ignored during backpropagation. As a result the network learns to predict a single body configuration.

The implementation of our model is in MatConvNet [36] and our code will be publicly available. In the next section, we evaluate the components of the recurrent human model, examine how well the regressed heatmaps address the problem of occlusion detection and compare our results with related approaches.

4 Experiments

We evaluate the components of our model and compare with related methods for the task of 2D human pose estimation from a single image. The evaluation is based on the MPII Human Pose [1] and extended LSP [19] datasets. On the MPII Human Pose [1] dataset, we evaluate for single human pose estimation, while the LSP [19] dataset includes labels only for single human evaluation. Keypoint annotation is provided for both datasets, 16 keypoints in MPII Human Pose (Fig. 2) and 14 in LSP, which we use for generating the target ground-truth keypoint and body part heatmaps for training. The parameters of the model,

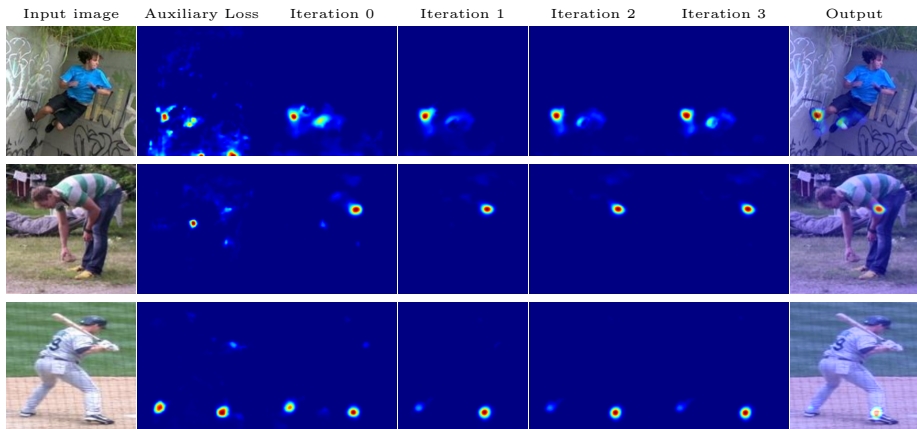


Fig. 5. More Results from the LSP dataset: We visualize the predicted heatmaps after every iteration of our recurrent module for the right ankle (*first row*), left elbow (*second row*) and right ankle (*third row*).

such as the learning rate and number of training epochs, are defined based on the validation dataset of MPII Human Pose, as proposed by [32], and remain the same for all evaluations. Moreover, the validation dataset of [32] is used for all the baseline evaluations. Our network architecture is significantly different from the common recognition models [20,30] and thus we choose to train from scratch instead of fine-tuning a pre-learned model.

The evaluation of the recurrent human model is divided into three parts: the component evaluation, occlusion evaluation and comparison with related methods. The different parts of our model are examined in the model components evaluation. In the occlusion part, we evaluate the potential of our model to predict whether a keypoint is visible. Finally, we compare our model with related methods, mainly deep learning approaches. The main performance metric for the evaluations is the PCKh measurec [1]. Based on the PCKh definition, a keypoint is correctly localized if the distance between the predicted and ground-truth keypoint is smaller than 50% of the head length.

4.1 Component Evaluation

The proposed model is composed of different objectives and the recurrent module, where the recurrent module can include several iterations. In this evaluation, we investigate the contribution of each component to the final performance. For this purpose, we rely on the MPII Human Pose [1] dataset with the validation dataset from [32]. The results of the component evaluation are summarized in Table 1.

At first, we evaluate the objective of the keypoint heatmaps (first row, Table 1). This evaluation composes the baseline of the proposed model. Next, the

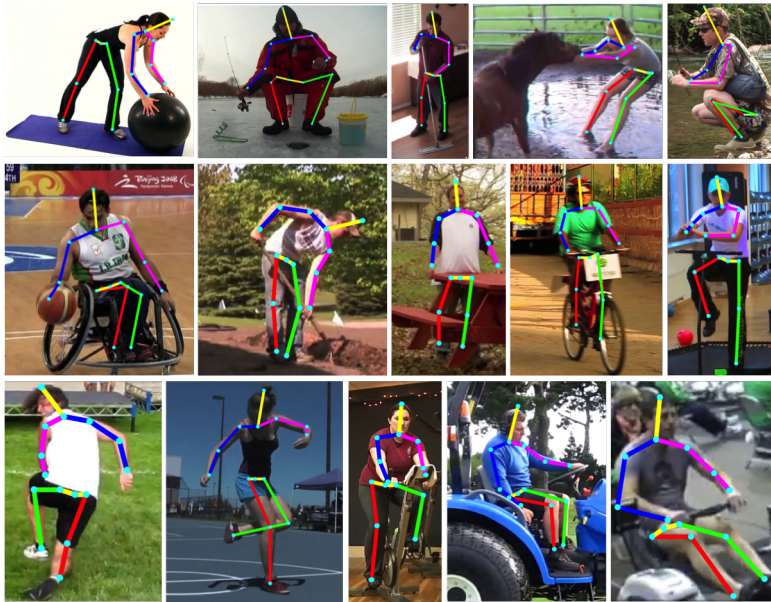


Fig. 6. Pose Results on MPII Human Pose: the predictions are from three iterations of the recurrent module.

second objective of the keypoint heatmaps is included in the evaluation (second row, Table 1). We do not aim to predict body parts, but observe that this additional objectives is helpful for capturing additional body constraints and thus it brings a (small) boost to the model performance. After the objectives' evaluation, we include the recurrent module performance. Training the model with 1 iteration (third row, Table 1) improves the results around 2%. In our experimentation, we observed that inserting another iteration in the model training does not result in better performance. Similarly, including another iteration during inference (fourth row, Table 1) does not boost the performance. In general, the parts that are already well predicted using our feed-forward model benefit less from the recurrent module (e.g. head). Finally, we noticed that 2 iterations in total are sufficient for a stable performance in all evaluations. Although, we choose to have a global model for the iterations, individual number of iterations can be chosen for each body part in order to improve the final outcome.

4.2 Occlusion Prediction

In this experiment, we analyse the potential of the heatmaps to predict the visibility of a keypoint. We argue that the heatmaps of occluded keypoints tend to have low responses (in terms of magnitude). As a result, the visibility of a keypoint can be inferred from the heatmap responses. For that purpose, we evaluate the performance of our model on predicting whether a keypoint is visible or

Table 1. Model Components: We evaluate the components of our model for the body keypoints on MPII Human Pose dataset using the PCKh metric and the validation dataset from [32]. The first row corresponds to the single objective performance, while in the second row the second objective is included to the model. In the third row, the model 2-objective model is additionally trained with the recurrent module for 1 iteration. The results for 2 and 3 iterations come by adding extra iterations during testing.

Heatmaps	Head	Shoulder	Elbow	Wrist	Hip	Knee	Ankle	PCKh
Keypoint	94.9	89.8	80.0	73.4	79.1	70.0	62.9	79.5
+ Body Part	94.8	90.5	80.6	72.7	80.0	71.3	65.2	80.1
+ 1 Iteration	95.6	91.2	81.9	74.5	81.8	73.9	67.3	81.6
+ 2 Iterations	95.5	91.3	81.8	74.4	81.5	74.1	67.9	81.6

occluded. The evaluation is performed on the validation set of the MPII Human Pose dataset which provides occlusion labels. However, the distribution of visible and occluded keypoints is unbalanced (only $\sim 23\%$ of annotated keypoints are tagged as occluded). For this reason we separate the keypoints into visible and occluded sets, and report predictions for each set separately. For the visibility prediction, the visible keypoints form the positive class and a Precision-Recall curve is computed based on the maximum heatmap response. On the other hand, for the occlusion prediction, the occluded keypoints compose the positive class and the Precision-Recall curve is again computed based on the maximum heatmap responses of the predictions and the ground-truth labels.

This experiment is performed using the two training scenarios that were defined in Sec. 2.5. In the first case, the occluded keypoints and body parts are ignored from the ground-truth labels, while in the second case, the heatmap regions of the occluded keypoints are penalized and thus forced to converge to zero. Our results for both visibility and occlusion prediction are summarized in Fig. 7. Note that we do not compare with another approach since we are not aware of any related method that performs occlusion detection on this dataset. One can see that the model with penalized occluded keypoints (in the training process) performs better than our standard model that ignores occluded keypoints and body parts. In practice, we observe that the network learns to treat areas of occluded keypoints as background (see Fig. 8). Nevertheless, we found out that the overall performance of the network that penalizes occluded keypoints from training is around 3% worse than then network that ignores the occluded keypoints. Our average precision (AP) is more than 90% for the case of the visibility prediction, but lower for the occlusion prediction. Our results are not direct comparable to the 35% of average detection accuracy of occluded joint from [26] or the 85% of accuracy of occlusion prediction from [10]; but these evaluations are indicative that our performance is good for this problem.

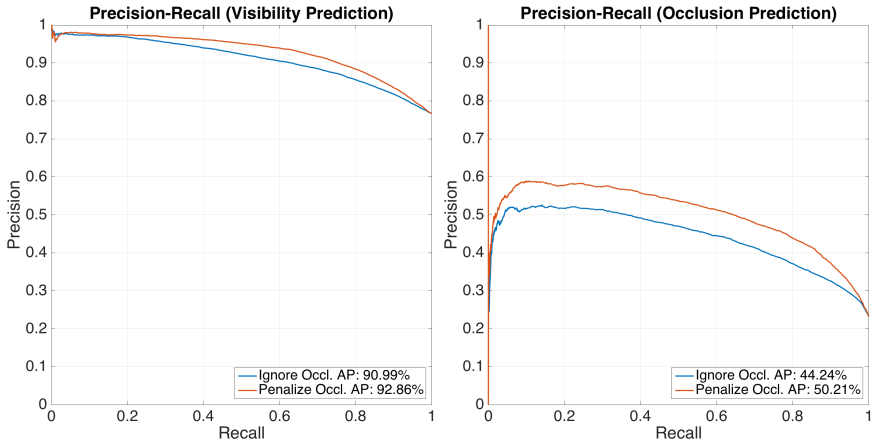


Fig. 7. Visibility and Occlusion Prediction: The precision-recall curve for the visibility prediction (left) and occlusion prediction (right) curves. The evaluation is performed using two different models: the first model is trained by ignoring the occluded keypoints (*Ignore Occl.*) during training and the second model by penalizing them (*Penalize Occl.*) and thus treating them as background. The average precision (AP) is reported for both training scenarios.



Fig. 8. Visibility Heatmaps: On the left, the predicted *right ankle* heatmap is visualized for the model that ignores the occluded keypoints during training, while on the right the same heatmap is presented for the model that penalizes the occluded keypoints (during training). The right heatmap response is low for the occluded keypoint because the model has learnt not to give high responses at the occluded area. On the other hand, the model that ignores the occluded keypoints, during training, makes predictions about the ankle location based on the context.

4.3 Comparison with other Methods

In our last experiment, we compare our results with related methods on MPI Human Pose [1] and LSP [19] datasets. In both evaluations, our model is executed for three iterations. We do not use any ground-truth information for the localization of the individuals in the LSP dataset, while rough localization is provided for the MPI Human Pose dataset.

MPII Human Pose Dataset. We use the same training and validation protocol as [32]. Our results are summarized in Table 2 and also samples are visualized in Fig. 6. In all cases, we achieve on par performance with other methods. It is worth noting that our model architecture is significantly simpler than [32] and it does not depend on a graphical model inference as [33]. One should also observe that our model performs better to the iterative method of Carreira *et al.* [8] which relies on a pre-trained model and training in stages.

Table 2. MPII Human Pose Evaluation. The PCKh measure is used for the evaluation. The scores are reported for each keypoint separately and for the whole body. The area under the curve (AUC) is also reported.

Ours	Head	Shoulder	Elbow	Wrist	Hip	Knee	Ankle	Total	AUC
	97.2	92.6	84.6	78.4	83.7	75.7	70.0	83.9	55.5
Tompson et al. [33]	95.8	90.3	80.5	74.3	77.6	69.7	62.8	79.6	51.8
Carreira et al. [8]	95.7	91.7	81.7	72.4	82.8	73.2	66.4	81.3	49.1
Tompson et al. [32]	96.1	91.9	83.9	77.8	80.9	72.3	64.8	82.0	54.9
Pishchulin et al. [24]	94.1	90.2	83.4	77.3	82.6	75.7	68.6	82.4	56.5
Wei et al. [38]	97.7	94.5	88.3	83.4	87.9	81.9	78.3	87.9	60.8

LSP Dataset. The dataset is composed of 2000 images, where half of the images are used for training (Fig 9). There is also the extension of LSP [19] with 10000 training samples which we use for this experiment. However, we observe that the training data is not sufficient for training our model from scratch, and thus we merge the training data of the extended LSP with the MPII Human Pose dataset. We also report results using a model trained or fine-tuned on the MPII Human Pose dataset. Our results are presented in Table 3. The evaluation is accomplished using the PCK measure (threshold at 0.2) that is similar to PCKh, but it has a reference part the length of the torso instead of the head. It is clear that we achieve promising performance for all keypoints. In particular, our recurrent human model performs better than the iterative method of Carreira *et al.* [8], as well as, the graph-based model with deep body part detectors of Chen & Yuille [9].

Table 3. LSP Evaluation. The PCK measure is used for the evaluation. The scores are reported for each keypoint separately and for the whole body. We report results using the trained model from MPII Human Pose, the MPII model fine tuned on the extended LSP training data, and also training a new model by combining the training data of the MPII Human Pose with the extended LSP dataset.

	Head	Shoulder	Elbow	Wrist	Hip	Knee	Ankle	Total
Ours (MPII model)	90.8	84.4	76.3	70.4	81.5	81.9	77.8	80.5
Ours (fine-tuned on MPII model)	94.3	87.1	78.6	72.0	78.1	83.2	77.1	81.5
Ours (MPII & LSP data, 1 iteration)	95.6	88.8	80.7	75.5	83.0	86.2	80.6	84.3
Ours (MPII & LSP data, 2 iterations)	95.2	88.7	81.7	76.8	83.8	86.7	82.5	85.1
Pishchulin et al. [23]	87.2	56.7	46.7	38.0	61.0	57.5	52.7	57.1
Wang Li et al. [37]	84.7	57.1	43.7	36.7	56.7	52.4	50.8	54.6
Carreira et al. [8]	90.5	81.8	65.8	59.8	81.6	70.6	62.0	73.1
Chen & Yuille [9]	91.8	78.2	71.8	65.5	73.3	70.2	63.4	73.4
Fan et al. [12]	92.4	75.2	65.3	64.0	75.7	68.3	70.4	73.0
Pishchulin et al. [24]	97.0	91.0	83.8	78.1	91.0	86.7	82.0	87.1



Fig. 9. Pose Results on LSP Dataset: the result after three iterations in the recurrent module.

5 Conclusion

We have introduced the recurrent human model for 2D human pose estimation. Our model is composed of a ConvNet with a recurrent module for human pose estimation. The recurrent model captures context iteratively, resulting in improved localization performance. Moreover, the recurrent human model can be trained end-to-end and does not require a pre-trained network to achieve good performance. We demonstrate state-of-the-art performance on two challenging human pose estimation datasets, training the model from scratch. Finally, the regressed heatmaps can be useful for predicting occlusion of keypoints.

Future work will investigate whether the heat map obtained by combining the keypoints and body parts (shown in Fig. 2(c)) can be used to avoid erroneous keypoint predictions (such as left/right hand swapping).

References

1. Andriluka, M., Pishchulin, L., Gehler, P., Schiele, B.: 2d human pose estimation: New benchmark and state of the art analysis. In: *Computer Vision and Pattern Recognition (CVPR)*, 2014 IEEE Conference on. pp. 3686–3693. IEEE (2014)
2. Andriluka, M., Roth, S., Schiele, B.: Pictorial structures revisited: People detection and articulated pose estimation. In: *Computer Vision and Pattern Recognition*, 2009. CVPR 2009. IEEE Conference on. pp. 1014–1021. IEEE (2009)
3. Belagiannis, V., Amin, S., Andriluka, M., Schiele, B., Navab, N., Ilic, S.: 3D pictorial structures for multiple human pose estimation. In: *IEEE Computer Society Conference on Computer Vision and Pattern Recognition (CVPR)*. IEEE (June 2014)
4. Belagiannis, V., Rupprecht, C., Carneiro, G., Navab, N.: Robust optimization for deep regression. In: *International Conference on Computer Vision (ICCV)*. IEEE (December 2015)
5. Bottou, L.: Large-scale machine learning with stochastic gradient descent. In: *Proceedings of COMPSTAT'2010*, pp. 177–186. Springer (2010)
6. Bourdev, L., Malik, J.: Poselets: Body part detectors trained using 3d human pose annotations. In: *IJCV* (2009)
7. Buehler, P., Everingham, M., Huttenlocher, D.P., Zisserman, A.: Upper body detection and tracking in extended signing sequences. *IJCV* 95(2), 180–197 (2011)
8. Carreira, J., Agrawal, P., Fragkiadaki, K., Malik, J.: Human pose estimation with iterative error feedback. *arXiv preprint arXiv:1507.06550* (2015)
9. Chen, X., Yuille, A.L.: Articulated pose estimation by a graphical model with image dependent pairwise relations. In: *Advances in Neural Information Processing Systems*. pp. 1736–1744 (2014)
10. Chen, X., Yuille, A.L.: Parsing occluded people by flexible compositions. In: *Proceedings of the IEEE Conference on Computer Vision and Pattern Recognition*. pp. 3945–3954 (2015)
11. Eichner, M., Marin-Jimenez, M., Zisserman, A., Ferrari, V.: 2d articulated human pose estimation and retrieval in (almost) unconstrained still images. *IJCV* 99, 190–214 (2012)
12. Fan, X., Zheng, K., Lin, Y., Wang, S.: Combining local appearance and holistic view: Dual-source deep neural networks for human pose estimation. In: *Computer*

- Vision and Pattern Recognition (CVPR), 2015 IEEE Conference on. pp. 1347–1355. IEEE (2015)
13. Felzenszwalb, P., Huttenlocher, D.: Pictorial structures for object recognition. *IJCV* 61(1) (2005)
 14. Ferrari, V., Marin-Jimenez, M., Zisserman, A.: Progressive search space reduction for human pose estimation. In: *Computer Vision and Pattern Recognition, 2008. CVPR 2008. IEEE Conference on*. pp. 1–8. IEEE (2008)
 15. Fischler, M., Elschlager, R.: The representation and matching of pictorial structures. *IEEE Transactions on Computer c-22*(1), 67–92 (Jan 1973)
 16. Gkioxari, G., Hariharan, B., Girshick, R., Malik, J.: Using k-poselets for detecting people and localizing their keypoints. In: *Proceedings of the IEEE Conference on Computer Vision and Pattern Recognition*. pp. 3582–3589 (2014)
 17. Ioffe, S., Szegedy, C.: Batch normalization: Accelerating deep network training by reducing internal covariate shift. *arXiv preprint arXiv:1502.03167* (2015)
 18. Jain, A., Tompson, J., LeCun, Y., Bregler, C.: Modeep: A deep learning framework using motion features for human pose estimation. In: *Computer Vision-ACCV 2014*, pp. 302–315. Springer (2014)
 19. Johnson, S., Everingham, M.: Learning effective human pose estimation from inaccurate annotation. In: *Proceedings of IEEE Conference on Computer Vision and Pattern Recognition* (2011)
 20. Krizhevsky, A., Sutskever, I., Hinton, G.E.: Imagenet classification with deep convolutional neural networks. In: *Advances in neural information processing systems*. pp. 1097–1105 (2012)
 21. Oberweger, M., Wohlhart, P., Lepetit, V.: Hands deep in deep learning for hand pose estimation. *arXiv preprint arXiv:1502.06807* (2015)
 22. Pfister, T., Charles, J., Zisserman, A.: Flowing convnets for human pose estimation in videos. In: *Proc. ICCV* (2015)
 23. Pishchulin, L., Andriluka, M., Gehler, P., Schiele, B.: Strong appearance and expressive spatial models for human pose estimation. In: *Proceedings of the IEEE International Conference on Computer Vision*. pp. 3487–3494 (2013)
 24. Pishchulin, L., Insafutdinov, E., Tang, S., Andres, B., Andriluka, M., Gehler, P., Schiele, B.: Deepcut: Joint subset partition and labeling for multi person pose estimation. *arXiv preprint arXiv:1511.06645* (2015)
 25. Pishchulin, L., Jain, A., Andriluka, M., Thormählen, T., Schiele, B.: Articulated people detection and pose estimation: Reshaping the future. In: *Computer Vision and Pattern Recognition (CVPR), 2012 IEEE Conference on*. pp. 3178–3185. IEEE (2012)
 26. Rafi, U., Gall, J., Leibe, B.: A semantic occlusion model for human pose estimation from a single depth image. In: *Proceedings of the IEEE Conference on Computer Vision and Pattern Recognition Workshops*. pp. 67–74 (2015)
 27. Ross, S., Munoz, D., Hebert, M., Bagnell, J.A.: Learning message-passing inference machines for structured prediction. In: *Computer Vision and Pattern Recognition (CVPR), 2011 IEEE Conference on*. pp. 2737–2744. IEEE (2011)
 28. Rumelhart, D.E., Hinton, G.E., Williams, R.J.: Learning representations by back-propagating errors. *Cognitive modeling* 5 (1988)
 29. Sapp, B., Toshev, A., Taskar, B.: Cascaded models for articulated pose estimation. In: *Computer Vision-ECCV 2010*, pp. 406–420. Springer (2010)
 30. Simonyan, K., Zisserman, A.: Very deep convolutional networks for large-scale image recognition. *arXiv preprint arXiv:1409.1556* (2014)

31. Szegedy, C., Liu, W., Jia, Y., Sermanet, P., Reed, S., Anguelov, D., Erhan, D., Vanhoucke, V., Rabinovich, A.: Going deeper with convolutions. In: Proceedings of the IEEE Conference on Computer Vision and Pattern Recognition. pp. 1–9 (2015)
32. Tompson, J., Goroshin, R., Jain, A., LeCun, Y., Bregler, C.: Efficient object localization using convolutional networks. In: Proceedings of the IEEE Conference on Computer Vision and Pattern Recognition. pp. 648–656 (2015)
33. Tompson, J.J., Jain, A., LeCun, Y., Bregler, C.: Joint training of a convolutional network and a graphical model for human pose estimation. In: Advances in neural information processing systems. pp. 1799–1807 (2014)
34. Toshev, A., Szegedy, C.: Deeppose: Human pose estimation via deep neural networks. In: Proceedings of the IEEE Conference on Computer Vision and Pattern Recognition. pp. 1653–1660 (2014)
35. Tu, Z., Bai, X.: Auto-context and its application to high-level vision tasks and 3d brain image segmentation. *Pattern Analysis and Machine Intelligence, IEEE Transactions on* 32(10), 1744–1757 (2010)
36. Vedaldi, A., Lenc, K.: Matconvnet – convolutional neural networks for matlab. In: Proceeding of the ACM Int. Conf. on Multimedia (2015)
37. Wang, F., Li, Y.: Beyond physical connections: Tree models in human pose estimation. In: Proceedings of the IEEE Conference on Computer Vision and Pattern Recognition. pp. 596–603 (2013)
38. Wei, S.E., Ramakrishna, V., Kanade, T., Sheikh, Y.: Convolutional pose machines. arXiv preprint arXiv:1602.00134 (2016)
39. Yang, Y., Ramanan, D.: Articulated pose estimation with flexible mixtures-of-parts. In: Computer Vision and Pattern Recognition (CVPR), 2011 IEEE Conference on. pp. 1385–1392. IEEE (2011)